

# Number counts in homogeneous and inhomogeneous dark energy models

N. J. Nunes<sup>1</sup>, A. C. da Silva<sup>2,3</sup> and N. Aghanim<sup>2</sup>

<sup>1</sup> School of Physics and Astronomy, 116 Church Street S.E., University of Minnesota, Minneapolis, Minnesota 55455, U.S.A.

<sup>2</sup> IAS-CNRS, Bâtiment 121, Université Paris Sud, F-91405, Orsay, France

<sup>3</sup> Centro de Astrofísica da Universidade do Porto, Rua das Estrelas, 4150-764 Porto, Portugal

October 16, 2018

**Abstract.** In the simple case of a constant equation of state, redshift distribution of collapsed structures may constrain dark energy models. Different dark energy models having the same energy density today but different equations of state give quite different number counts. Moreover, we show that introducing the possibility that dark energy collapses with dark matter (“inhomogeneous” dark energy) significantly complicates the picture. We illustrate our results by comparing four dark energy models to the standard  $\Lambda$ -model. We investigate a model with a constant equation of state equal to  $-0.8$ , a phantom energy model and two scalar potentials (built out of a combination of two exponential terms). Although their equations of state at present are almost indistinguishable from a  $\Lambda$ -model, both scalar potentials undergo quite different evolutions at higher redshifts and give different number counts. We show that phantom dark energy induces opposite departures from the  $\Lambda$ -model as compared with the other models considered here. Finally, we find that inhomogeneous dark energy enhances departures from the  $\Lambda$ -model with maximum deviations of about 15% for both number counts and integrated number counts. Larger departures from the  $\Lambda$ -model are obtained for massive structures which are rare objects making it difficult to statistically distinguish between models.

**Key words.** cosmology – galaxies: clusters

## 1. Introduction

In the present general picture of cosmology, converging evidences suggest that the matter density parameter is low and that the largest fraction of the energy density of the universe has an unknown nature leading to an accelerating phase. These indications come primarily from supernovae Ia data (e.g. Riess *et al.* (1998); Perlmutter *et al.* (1999); Riess *et al.* (2004)) and are corroborated by cosmic microwave background radiation (e.g. Spergel *et al.* (2003)) and large scale structure observations (e.g. Cole *et al.* (2005)), although there are different interpretations for the data (e.g. Blanchard *et al.* (2003); Shanks (2004)). A cosmological constant can explain the acceleration of the universe, however, the disagreement by  $\sim 120$  orders of magnitudes with predictions from theoretical particle physics has shown the need for resorting to an alternative explanation. This is why several theoretical models were recently proposed to explain this dark energy in the universe. This new component can be identified with a slowly varying, self-interacting, neutral scalar “quintessence” field (Wetterich (1988); Ratra and Peebles (1988); Ferreira and Joyce (1997); Zlatev *et al.* (1999))

which can be minimally coupled, non-minimally coupled (e.g. Uzan (1999); Amendola (2000); Baccigalupi *et al.* (2000)), a phantom (e.g. Caldwell (1999)), a tachyon (e.g. Bagla *et al.* (2003)) or of purely kinetic nature (e.g. Armendariz-Picon *et al.* (2000)), known as K-essence. An alternative to dark energy is a fluid with a Chaplygin gas type of equation of state (e.g. Kamenshchik *et al.* (2001)). See Sahni (2004) and references therein for a review on some of these, and other, models.

Regardless of its nature, dark energy as a dominant component, plays a role in the structure formation and thus is likely to modify the number of formed structures. The evolution of linear perturbations in a scalar field like quintessence and the effects on structure formation have already been investigated theoretically (e.g. Ferreira and Joyce (1997); Perrotta and Baccigalupi (2002); Amendola (2003)). The effects on the abundance of collapsed structures and its evolution with redshift were also widely explored and suggested as a tool to constrain the dark energy’s nature and evolution (e.g. Haiman *et al.* (2001); Weller *et al.* (2002); Weinberg and Kamionkowski

(2002); Battye and Weller (2003); Wang *et al.* (2004); Mohr (2004); Horellou and Berge (2005)).

Recently, numerical simulations including a dark energy component were performed by several groups to complement the analytical computations and to study the effects of dark energy at the structure level (e.g. shape of the dark matter halo, mass function) (Linder and Jenkins (2003); Lokas *et al.* (2003); Klypin *et al.* (2003); Kuhlen *et al.* (2004)). In such studies, the scalar field associated with dark energy is assumed not to have density fluctuations on scales of galaxy clusters or below. If dark energy influences the perturbations on small scales as proposed for example by Arbey *et al.* (2001), Bean and Magueijo (2002), Padmanabhan and Choudhury (2002) or Bagla *et al.* (2003), the collapse of structures as well as their properties will be affected.

Mota and van de Bruck (2004) have shown that the properties of collapsed halos (density contrast, virial radius) depend strongly on the shape of the potential, the initial conditions, the time evolution of the equation of state and *on the behaviour of the scalar field in non-linear regions*. This is what we will refer to as the *inhomogeneity* of the scalar field. More recently, Nunes and Mota (2004) have investigated how inhomogeneous quintessence models have a specific signature even in the linear regime of structure formation. They have shown that the time of collapse is affected by the inhomogeneity of dark energy and they have computed the resulting effect on the linearly extrapolated density threshold  $\delta_c$ . Moreover, they examined the evolution of matter overdensity as a function of time varying equation of state in homogeneous and inhomogeneous assumptions. Maor and Lahav (2005) have generalized the formalism to allow for a smooth transition between the homogeneous and inhomogeneous scenarios. They have concluded that, if only matter virializes, the final size of the system is fundamentally distinct from the one reached if the full system virializes.

In the present study, we extend the work of Nunes and Mota (2004) to investigate how the quintessence field affects the abundance of collapsed halos when the field follows the background evolution (homogeneous) and more specifically when it collapses with the dark matter (inhomogeneous). We compare the two assumptions for models with constant equation of state and more general cases of time-varying equation of state. To compute the structure abundances and their evolution with redshift, we use the canonical Press and Schechter (1974) formalism. Its theoretical expression allows us to account for the effects of inhomogeneous quintessence field through  $\delta_c$ , the growth factor as well as the volume element. Finally, we focus on the effects of the different models for structures with masses ranging between  $10^{13}$  and  $10^{16} h^{-1} M_\odot$ .

This paper is organised as follows. In Section 2 we introduce the fundamental equations that describe the evolution of the quintessence field and the collapse of structure in the homogeneous and inhomogeneous hypothesis.

In Section 3 we describe the method used to compute the number density of collapsed objects (mass function) in both of these scenarios, including the case where the equation of state of dark energy is allowed to vary with time. We give results and discuss the effects of the normalisation of the mass function on the predicted number counts in Section 4, and present concluding remarks in Section 5.

## 2. Theoretical background

In a spatially flat Friedmann-Robertson-Walker Universe the cosmic dynamics is determined by a background pressureless fluid (dark and visible matter), radiation and dark energy. The governing equations of motion are

$$\dot{H} = -\frac{\kappa^2}{2}(\rho_B + p_B + \rho_{de} + p_{de}), \quad (1)$$

$$\dot{\rho}_B = -3H(\rho_B + p_B), \quad (2)$$

$$\dot{\rho}_{de} = -3H(\rho_{de} + p_{de}), \quad (3)$$

with

$$H^2 = \frac{\kappa^2}{3}(\rho_B + \rho_{de}). \quad (4)$$

Here  $H = \dot{a}/a$  is the expansion rate of the Universe,  $a(t)$  is the scale factor,  $\kappa^2 = 8\pi G$  and  $\rho_B$  and  $p_B$  are the energy density and pressure of the background fluid, respectively. In this work the background is taken to be dominated by non-relativistic matter, hence,  $\rho_B = \rho_m \propto a^{-3}$ . If dark energy is a perfect fluid its energy density and pressure are related by the equation of state  $\rho_{de} = w\rho_{de}$  and  $\rho_{de} = \Omega_{de}\rho_0/a^{3(w+1)}$ . Alternatively, dark energy can be described by a dynamical evolving scalar field rolling down its potential  $V(\phi)$ . In this case, its energy density and pressure are defined as,  $\rho_\phi = \dot{\phi}^2/2 + V$  and  $p_\phi = \dot{\phi}^2/2 - V$ , respectively where the relation  $w = p_\phi/\rho_\phi$ , still holds. The equation of motion for the scalar field is,

$$\ddot{\phi} = -3H\dot{\phi} - \frac{dV}{d\phi}. \quad (5)$$

We explore models of dark energy that have a significant contribution at high redshift unlike models such as the inverse power law (Zlatev *et al.* (1999)) or SUGRA models (Brax and Martin (1999)). We compare the results of such models with the cosmological constant model with  $w = -1$  and we assume  $\Omega_{de} = 0.7$  today for all models considered in the present study. Moreover, we choose the present value of the equation of state,  $w_0$ , and its running,  $dw/dz(z=0)$ , to be within the current observational limits (Riess *et al.* (2004)).

Figure 1 shows the evolution of the dark energy density and equation of state with redshift for the models we consider in this paper. We focus on dark energy models for which  $w = -0.8$ ,  $w = -1.2$  (phantom energy, Caldwell (1999)) and two cases where the dark energy results from a slowly evolving scalar field in a potential with two exponential terms (2EXP) (Barreiro *et al.* (2000))

$$V(\phi) = V_0 (e^{\alpha\kappa\phi} + e^{\beta\kappa\phi}). \quad (6)$$

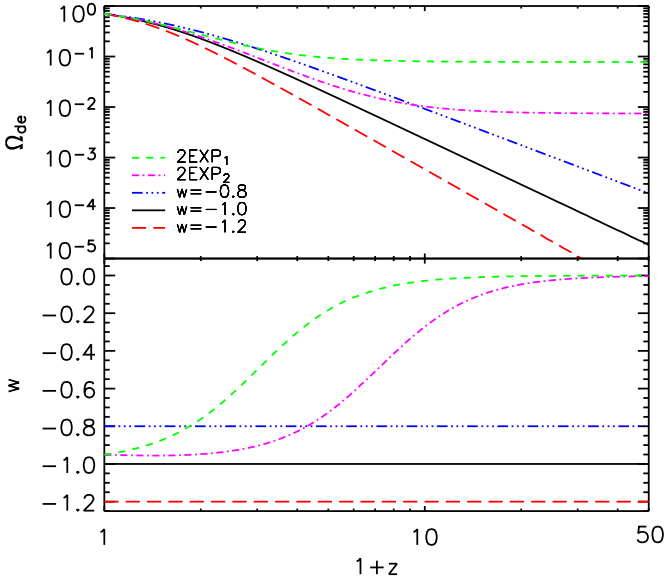


**Fig. 1.** Evolution of the dark energy density (top panel) and equation of state (bottom panel) with redshift for the models considered in this paper:  $w = -1$  (solid line),  $w = -1.2$  (long dashed line),  $w = -0.8$  (triple dot-dashed line), 2EXP<sub>1</sub> ( $\alpha, \beta$ ) = (6.2, 0.1) (dashed line), and 2EXP<sub>2</sub> ( $\alpha, \beta$ ) = (20.1, 0.5) (dot-dashed line).

We choose as in Nunes & Mota (2004) the pairs  $(\alpha, \beta) = (6.2, 0.1)$  (2EXP<sub>1</sub>) and  $(\alpha, \beta) = (20.1, 0.5)$  (2EXP<sub>2</sub>). Both provide an equation of state at present  $w_0 = -0.95$ . The equation of state for 2EXP<sub>1</sub> approaches zero faster than for 2EXP<sub>2</sub> (see bottom panel in Fig. 1). The two models differ also by their contributions at high redshift. As seen from top panel of Fig. 1, 2EXP<sub>1</sub> provides a contribution of dark energy that is non negligible at high redshifts ( $\Omega_\phi = 0.1$  at  $z = 5$  for 2EXP<sub>1</sub> whereas  $\Omega_\phi = 0.02$  for 2EXP<sub>2</sub> at same redshift).

In this work we use the spherical collapse model to describe the gravitational collapse of an overdense region of radius  $r$  and density contrast  $\delta$  such that  $1 + \delta = \rho_{m,c}/\rho_m = (a/r)^3$ , where  $\rho_{m,c}$  and  $\rho_m$  are the energy densities of pressureless matter in the cluster and in the background, respectively. We have considered the possibility that dark energy also clusters, i.e.  $\rho_{de,c} \neq \rho_{de}$ . Following Mota and van de Bruck (2004) and Nunes and Mota (2004), we study two extreme limits for the evolution of dark energy in the overdensity region. First, we assume that dark energy is “homogeneous”, i.e. the value of  $\rho_{de}$  inside the overdensity is the same as in the background. Second, dark energy is “inhomogeneous” and collapses with dark matter. In general terms, the evolution of dark energy inside a cluster can be written as in Mota and van de Bruck (2004)

$$\dot{\rho}_{de,c} = -3\frac{\dot{r}}{r}(\rho_{de,c} + p_{de,c}) + \Gamma_{de}, \quad (7)$$

where  $\Gamma_{de}$  represents the dark energy loss inside the cluster and the ratio  $\dot{r}/r$  is related to the Hubble ratio and the evolution of the density contrast through

$$\frac{\dot{r}}{r} = \frac{\dot{a}}{a} - \frac{1}{3} \frac{\dot{\delta}}{1 + \delta}. \quad (8)$$

If dark energy is homogeneous, then

$$\Gamma_{de} = -3 \left( \frac{\dot{a}}{a} - \frac{\dot{r}}{r} \right) (\rho_{de,c} + p_{de,c}). \quad (9)$$

However if dark energy is inhomogeneous and collapses with dark matter,  $\Gamma_{de} = 0$  and the equation of motion of a scalar field inside the cluster is

$$\ddot{\phi}_c = -3\frac{\dot{r}}{r}\dot{\phi}_c - \frac{dV(\phi_c)}{d\phi_c}. \quad (10)$$

Finally, the evolution of the linear density contrast  $\delta_L$  is determined by

$$\ddot{\delta}_L = -2H\dot{\delta}_L + \frac{\kappa^2}{2} [\rho_m \delta_L + (1 + 3w)\delta_{de} \rho_{de} + 3\rho_{de} \delta w], \quad (11)$$

where we have defined the linear density contrast in dark energy as  $\delta_{de} = \delta\rho_{de}/\rho_{de}$  and  $\delta w$  is the linear perturbation in the equation of state.

### 3. Mass function

In hierarchical models, cosmic structures form from the gravitational amplification of small initial density perturbations. The time evolution of the structure abundances is determined mainly by the rate at which the perturbations grow until they reach the collapse, or virialization.

An analytical computation, proposed by Press and Schechter (1974), gives the comoving number density of collapsed dark matter halos of mass  $M$  in the interval  $dM$  at a given redshift of collapse,  $z$  by

$$\frac{dn}{dM} = -\sqrt{\frac{2}{\pi}} \frac{\rho_{m0}}{M} \frac{\delta_c(z)}{\sigma(M, z)} \frac{d \ln \sigma(M, z)}{dM} \exp \left[ -\frac{\delta_c(z)^2}{2\sigma(M, z)^2} \right], \quad (12)$$

where  $\rho_{m0}$  is the present matter mean density of the universe and  $\delta_c(z)$  is the linearly extrapolated density threshold above which structures collapse, i.e.  $\delta_c(z) = \delta_L(z = z_{col})$ . In an Einstein-de Sitter Universe, an overdensity region collapses with a linear contrast  $\delta_c = 1.686$  (see e.g. Padmanabhan (1993)). This canonical value was used in the seminal paper of Press and Schechter (1974). The linearly extrapolated density threshold has recently been re-computed (Nunes & Mota 2004) in a more general case accounting for homogeneous and inhomogeneous dark energy. They show significant variations of  $\delta_c(z)$  with redshift and with dark energy models considered. In the present study, we compute halo abundances using the results on  $\delta_c(z)$  obtained by Nunes & Mota (2004), to which we refer the reader for further details.

The quantity  $\sigma(M, z) = g(z)\sigma_M$  is the linear theory *rms* density fluctuation in spheres of radius  $R$  containing the mass  $M$  and  $g(z) = \delta_L(z)/\delta_L(z=0)$  is the linear growth factor. The smoothing scale  $R$  is often specified by the mass within the volume defined by the window function at the present time (e.g. Peebles 1980). In our analysis the variance of the smoothed overdensity containing a mass  $M$  is given by

$$\sigma_M = \sigma_8 \left( \frac{M}{M_8} \right)^{-\gamma/3}, \quad (13)$$

where  $M_8 = 6 \times 10^{14} \Omega_m h^{-1} M_\odot$ , the mass inside a sphere of radius  $R_8 = 8h^{-1} \text{Mpc}$ , and  $\sigma_8$  is the variance of the overdensity field smoothed on a scale of size  $R_8$ . The index  $\gamma$  is a function of the mass scale and the shape parameter,  $\Gamma$ , of the matter power spectrum (Viana and Liddle (1996))

$$\gamma = (0.3\Gamma + 0.2) \left[ 2.92 + \frac{1}{3} \log \left( \frac{M}{M_8} \right) \right]. \quad (14)$$

In our study we use  $\Gamma = 0.167$  (Spergel et al. 2003).

For a fixed  $\sigma_8$  (power spectrum normalization) the predicted number density of dark matter halos given by the above formula is uniquely affected by the dark energy models through the ratio  $\delta_c(z)/g(z)$ . The underlying assumption of this approach is that the transfer function used in the computation of  $\sigma_M$  is that of a cosmological constant model. This is a good approximation at cluster scales for homogeneous dark energy models (Ma *et al.* (1999)), which remains to be theoretically investigated in the inhomogeneous hypothesis.

For a fixed local halo abundance, the important quantity to consider is thus  $\xi = \delta_c(z)/\sigma_8 g(z)$ . We have verified that apart from  $w = -1.2$  (phantom energy) all homogeneous models have a ratio  $\delta_c/\sigma_8 g$  below that of the  $\Lambda$ -model. This means that, at higher redshifts, models  $w = -0.8$ , 2EXP<sub>1</sub> and 2EXP<sub>2</sub> are expected to give larger halo densities (whereas the phantom energy model is expected to give lower abundances) when compared to the cosmological constant model. For inhomogeneous dark energy we find that all models, except the  $w = -0.8$  model, have larger  $\delta_c/\sigma_8 g$  than the cosmological constant model, and therefore we expect at high redshift lower halo densities for this models (higher abundances in the case of  $w = -0.8$ ) when compared to the  $\Lambda$ -model.

To obtain the same halo abundance at  $z = 0$  we scaled  $\sigma_8$  according to  $\sigma_8 = \delta_c(z=0)\sigma_{8,\Lambda}/\delta_{c,\Lambda}(z=0)$ , where the index ‘ $\Lambda$ ’ represents the cosmological constant model, and we fix  $\sigma_{8,\Lambda} = 0.9$ . Table 1 lists the values of  $\sigma_8$  obtained in this way. Note the much larger dispersion of  $\sigma_8$  between models in the inhomogeneous case (third column) as compared to homogeneous dark energy (second column) where models require practically the same  $\sigma_8$  to reproduce the present-day halo abundance of the  $\Lambda$ -model.

It is also interesting to see that the 2EXP<sub>1</sub> model requires the lowest and the  $w = -1.2$  model the highest  $\sigma_8$  normalizations to reproduce the same local abundance

**Table 1.** Variance of the overdensity field smoothed on  $8h^{-1} \text{Mpc}$  used in the normalization of number counts to the present-day halo abundance in  $\Lambda$ -model with  $\sigma_8 = 0.9$  for homogeneous (second column) and inhomogeneous (third column) dark energy models.

model	$\sigma_8$	
	homogeneous	inhomogeneous
2EXP <sub>1</sub>	0.897	0.876
2EXP <sub>2</sub>	0.899	0.886
$w = -0.8$	0.898	0.857
$w = -1.0$	0.900	0.900
$w = -1.2$	0.901	0.942

of halos. This means that structures form early, at a slow rate, if the universe is dominated by phantom dark energy. They form late, at a faster rate, in the 2EXP<sub>1</sub> model.

In Fig. 2 we plot the redshift evolution of the mass function of objects with mass  $10^{14} h^{-1} M_\odot$  for both homogeneous (top panel) and inhomogeneous (bottom panel) dark energy using Eq. (12). As discussed in the previous paragraphs the  $w = -0.8$ , 2EXP<sub>1</sub> and 2EXP<sub>2</sub> models give larger halo abundances than the  $w = -1$  model, whereas  $w = -1.2$  gives the lowest densities. We find this same qualitative behaviour within the mass range of interest for this paper,  $10^{13} - 10^{16} h^{-1} M_\odot$ , for both homogeneous and inhomogeneous dark energy models. The counts were normalized so that at  $z = 0$  all models give the same halo abundance as the cosmological constant ( $w = -1$ ) model gives for  $\sigma_8 = 0.9$ . Note that the overdensity contrast at collapse,  $\delta_c$ , is different for different dark energy models (see Fig. 2 in Nunes & Mota 2004) and therefore the number density of halos at  $z = 0$  is different if we assume the same  $\sigma_8$  for all models. The embedded panels in Fig. 2 show this situation (zoomed near  $z = 0$ ), where  $\sigma_8$  was set equal to 0.9 for all models. Larger differences are found in the case of inhomogeneous dark energy, because this is where  $\delta_c(z = 0)$  presents larger deviations from its value in a  $\Lambda$ -model (see Nunes & Mota 2004).

In what follows we assume the halo number densities of models normalized to the present-day halo abundance of the  $\Lambda$ -model. In Section 4.3 we discuss the effects of this assumption on our results.

## 4. Predicted number counts

In this paper we investigate the modifications caused by a dark energy component on the number of dark matter halos. We test for one model with a cosmological constant ( $w = -1$ ) and for four quintessence models (defined in Section 2). The computations are done in the case where dark energy is homogeneous and in the case where it may cluster, i.e. inhomogeneous dark energy. Moreover, we choose to explore the effects on the integrated number of dark matter halos in mass bins  $[M_{\text{inf}}, M_{\text{sup}}]$  illustrating different classes of cosmological structures, namely  $10^{13} - 10^{14}$ ,  $10^{14} - 10^{15}$ , and  $10^{15} - 10^{16}$  in units of  $h^{-1} M_\odot$ .

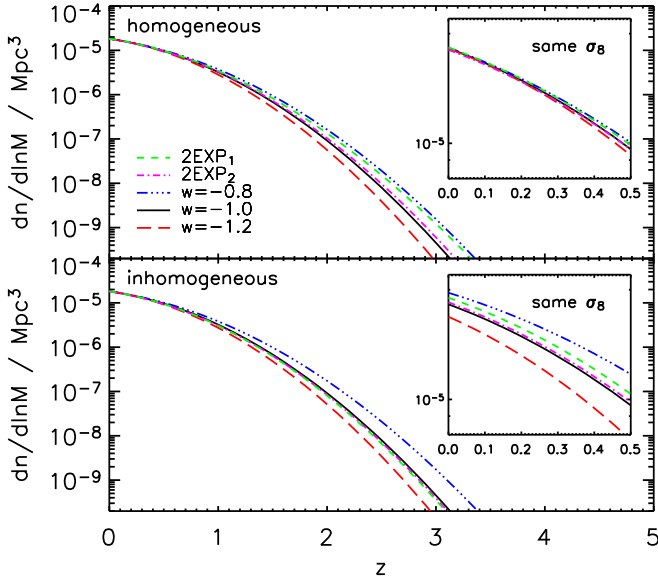


**Fig. 2.** Redshift evolution of the modified Press-Schechter mass function at  $M = 10^{14} h^{-1} M_{\odot}$  for homogeneous (top panel) and inhomogeneous (bottom panel) dark energy models. In the main panels models were normalized to reproduce the present-day abundance of dark matter halos of the  $\Lambda$ -model with  $\sigma_8 = 0.9$ . In the embedded panels models were normalized to the same  $\sigma_8 = 0.9$ . Lines are the same as for Fig. 1.

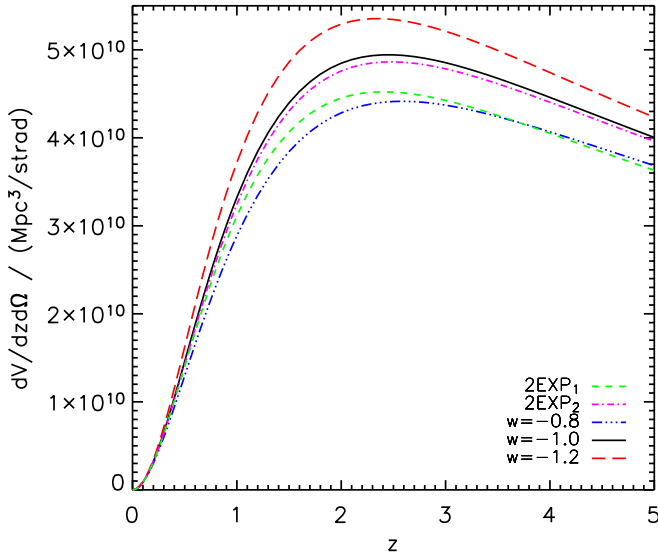


**Fig. 3.** Evolution of the volume element with redshift in both homogeneous (top panel) and inhomogeneous (bottom panel) dark energy scenarios. Lines are the same as for Fig. 1.

We study the effect of dark energy on the number of dark matter halos by computing two quantities. The first is the all sky number of halos per unit of redshift, in the mass bin

$$\mathcal{N}^{\text{bin}} \equiv \frac{dN}{dz} = \int_{4\pi} d\Omega \int_{M_{\text{inf}}}^{M_{\text{sup}}} \frac{dn}{dM} \frac{dV}{dz d\Omega} dM, \quad (15)$$

where the volume element is given by  $dV/dz d\Omega = r^2(z)/H(z)$ , with  $r(z) = \int_0^z H^{-1}(x) dx$ . The redshift evolution of  $dV/dz d\Omega$  for different models of dark energy is depicted in Fig. 3. Note that the volume element does not depend on the hypothesis of dark energy clustering, it is thus the same for both homogeneous and inhomogeneous dark energy models. Note also that the phantom model is the only one having a volume element larger than the volume element in the cosmological constant model.

The second quantity we compute is the all sky integrated number counts above a given mass threshold,  $M_{\text{inf}}$ , and up to redshift  $z$ :

$$N(z, M > M_{\text{inf}}) = \int_{4\pi} d\Omega \int_{M_{\text{inf}}}^{\infty} \int_0^z \frac{dn}{dM} \frac{dV}{dz' d\Omega} dM dz'. \quad (16)$$

Our knowledge of both these quantities for galaxy clusters will improve enormously with upcoming (underway or planned) cluster surveys operating at different wavebands. These include the Planck Surveyor satellite and South Pole Telescope (SPT) (Ruhl *et al.* (2004)) Sunyaev-Zel'dovich surveys, the XMM-Newton serendipitous X-ray cluster survey (XCS) (Romer *et al.* (2001)) and the recently proposed deep multiband optical Dark Energy Survey (DES) designed to probe almost the same sky region of SPT.

#### 4.1. Number counts in mass bins

Figures 4, 5 and 6 show the number counts,  $\mathcal{N}^{\text{bin}} = dN/dz$ , obtained from Eq. (15) (top panels) together with the difference of counts of the various dark energy models to the  $\Lambda$ -model,  $\Delta\mathcal{N}^{\text{bin}} = \mathcal{N}^{\text{bin}} - \mathcal{N}_{\Lambda}^{\text{bin}}$ , (bottom panels). First let us concentrate on the homogeneous dark energy case, i.e. on the left panels of these figures. Below redshift unity the volume element has the most important role in the integral of Eq. (15), as it increases by orders of magnitude. Above this redshift the volume element does not vary much and it is the mass function that decreases by orders of magnitude. It decreases faster for models of larger  $\delta_c/\sigma_8 g$ . Therefore, for our particular models, we expect to see at low redshifts, in decreasing order of number of counts per redshift, the following sequence of models:  $w = -1.2$ ,  $w = -1$ , 2EXP<sub>2</sub>, 2EXP<sub>1</sub> and  $w = -0.8$  and the reverse order at high redshifts. In practice this is only true if the maximum of counts occurs at a redshift around or greater than unity, i.e. after the volume element does not vary much. We can verify that this requirement is only satisfied in the lowest mass bin  $10^{13} < M/(h^{-1} M_{\odot}) < 10^{14}$ , hence the low redshift order might differ from the one stated in the two largest mass bins. Nonetheless, the high redshift description is accurate for all mass bins. More generally, the differences between counts can be understood in terms of the relative contribution to  $\mathcal{N}^{\text{bin}}$  of the integrand in Eq. (15). The counts thus depend not only on the volume element and on the growth factor but also on the small differences in  $\sigma_8$ . At high redshift, models with smaller  $\delta_c/\sigma_8 g$  ratios imply larger halo

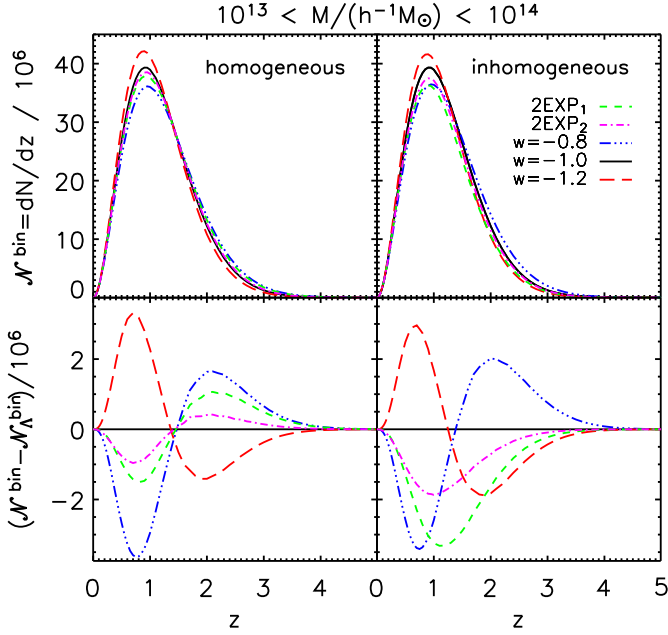


**Fig. 4.** Evolution of number counts (top panels) with redshift and differences from the  $w = -1$  (cosmological constant  $\Lambda$ ) model (bottom panels) for objects with mass within the range  $10^{13} < M/(h^{-1}M_{\odot}) < 10^{14}$ . Panels on the left show results for homogeneous dark energy whereas panels on the right show the same models in the inhomogeneous dark energy scenario. Lines are the same as for Fig. 1.

abundances and this effect dominates that of the volume element. At low redshifts the differences between counts from one model to another depend also on the masses of interest. As a matter of fact, the number of low mass structures is mostly sensitive to the volume element whereas for massive structures the number counts become sensitive to the normalisation  $\sigma_8$ . The left lower panels of the figures illustrate quantitatively the relative evolution of the number counts. For  $w = -1.2$ , the figures depict the expected excesses and deficits of counts compared to the cosmological constant model below and above redshift  $z_t$  (defined as  $\mathcal{N}^{\text{bin}}(z_t) = \mathcal{N}_{\Lambda}^{\text{bin}}(z_t)$ ). Conversely, we have deficits and excesses below and above  $z_t$ , respectively, for all the other models. It is also worth pointing out that larger mass bins imply a larger ratio  $\delta_c/\sigma$  (see Eq. (13)), which makes the mass function to dominate at lower redshifts in Eq. (15) and consequently  $z_t$  to move to smaller values as depicted in the figures.

Now, we turn to the comparison between the inhomogeneous and homogeneous hypotheses (right versus left panels in Figs. 4, 5 and 6). Figure 7 is helpful to understand how the differences arise. Indeed, when compared to the homogeneous case, we verify that the quantity  $\delta_c/\sigma_8 g$  is smaller in the inhomogeneous case for  $w = -0.8$  and larger for all the other models. Given this, it is clear that for  $w = -0.8$  we see, as expected, smaller deficits and larger excesses of counts comparatively to the homoge-

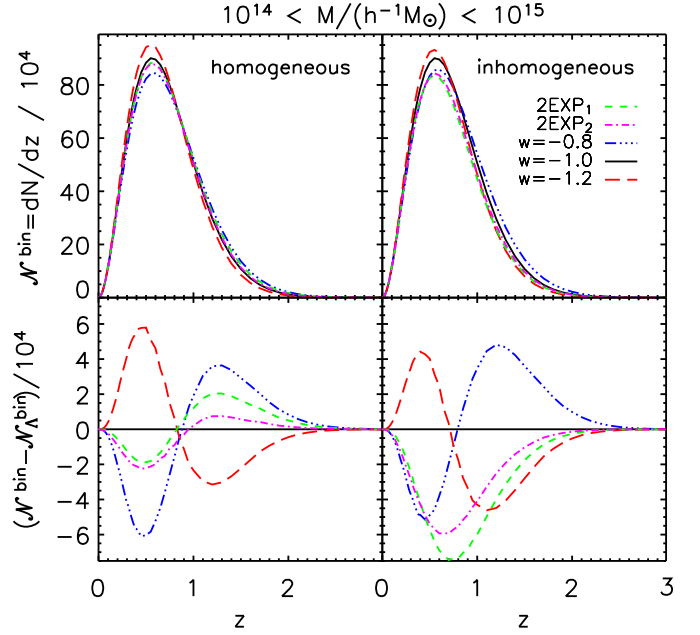


**Fig. 5.** Same as Fig. 4 for objects with mass within the range  $10^{14} < M/(h^{-1}M_{\odot}) < 10^{15}$ .

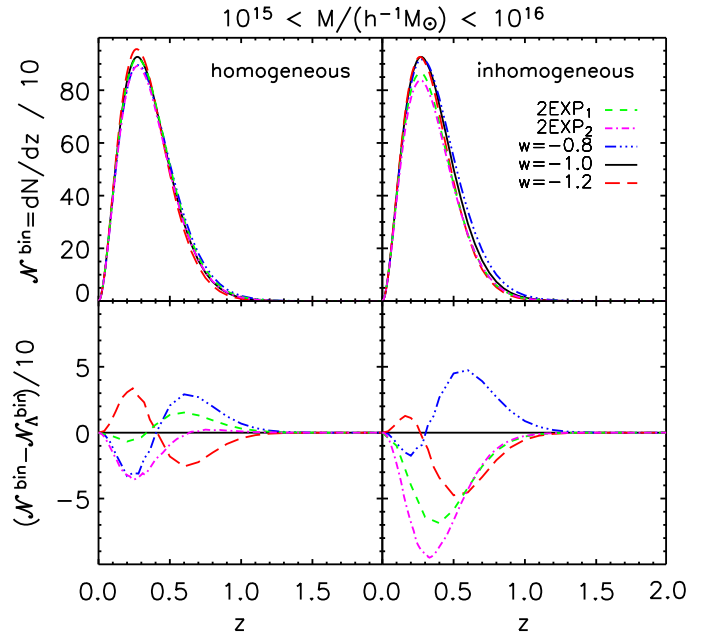


**Fig. 6.** Same as Fig. 4 for objects with mass within the range  $10^{15} < M/(h^{-1}M_{\odot}) < 10^{16}$ .

neous case and for all the other models the inverse trend. The effects of the inhomogeneous hypothesis are more evident for high mass bins where count deficits and excesses show larger differences between homogeneous and inhomogeneous dark energy. For example, in Fig. 6 we see that the  $w = -0.8$  model has  $\sim 2$  times larger count excess in the inhomogeneous case.

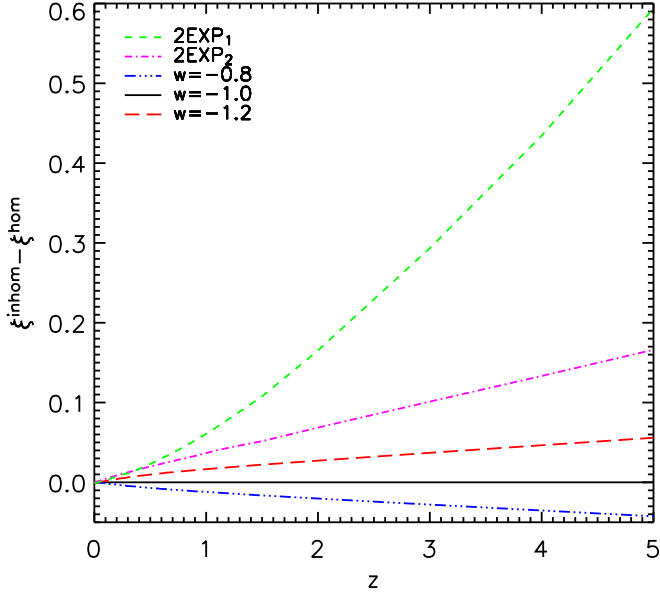


**Fig. 7.** Difference of  $\xi = \delta_c/g\sigma_8$  between inhomogeneous ( $\xi^{\text{inhom}}$ ) and homogeneous ( $\xi^{\text{hom}}$ ) dark energy models.

#### 4.2. Integrated number counts

The integrated number of collapsed structures above a given mass (Eq. (16)) is an important observable quantity. In this section we present results for the integrated number counts of structures with masses above  $M_{\text{inf}} = 10^{13}h^{-1}M_{\odot}$  and  $10^{14}h^{-1}M_{\odot}$ . These are displayed in the upper panels of Figs. 8 and 9, respectively (here we omit displaying results for  $M > M_{\text{inf}} = 10^{15}h^{-1}M_{\odot}$  because, as it will be clear below, integrated counts in this mass range can be directly estimated from the curves in Fig. 6). We also calculate the difference in integrated number counts with respect to the cosmological constant model shown in the lower panels of the same figures. As in the previous section, we compare the predicted numbers in the homogeneous (left panels of figures) and inhomogeneous hypotheses (right panels) for the cosmological models we consider in this study.

For each mass bin, the differences between integrated counts result from the combination of effects (that act on different mass ranges) discussed in the previous section. In our work we have obviously not performed the integration in the mass range in Eq. (16) all the way up to infinity but only to  $M_{\text{sup}} = 10^{16}h^{-1}M_{\odot}$ . In the cases  $M > M_{\text{inf}} = 10^{13}h^{-1}M_{\odot}$  and  $M > M_{\text{inf}} = 10^{14}h^{-1}M_{\odot}$ , integrated number counts reflect mainly the behaviour of curves in the lowest and middle mass bin, respectively. This is because  $N(z, M > M_{\text{inf}})$  is dominated by the contribution of the lower bound of the mass integration range. Hence, it is legitimate to concentrate on the lowest mass when a qualitative description of the integrated number counts is concerned.

We have seen in the Figs. 4, 5 and 6 that in the homogeneous case, the model with  $w = -1.2$  presents excesses with respect to the cosmological constant at low redshift

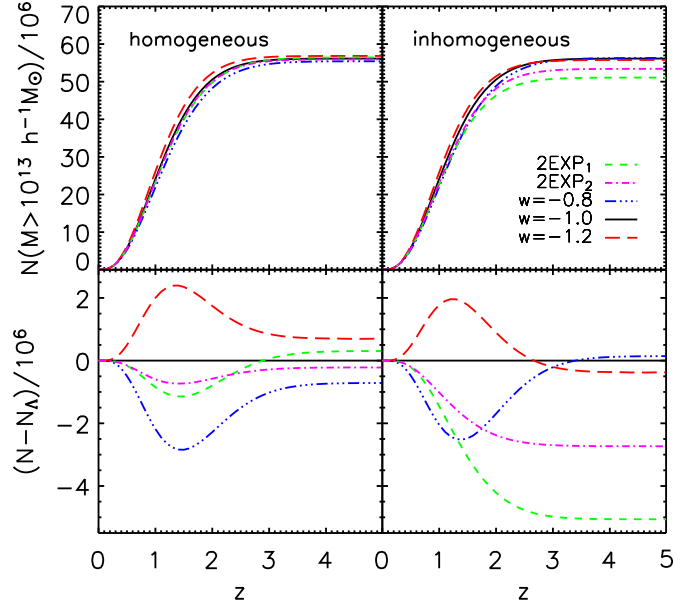


**Fig. 8.** Integrated number counts up to redshift  $z$  (top panels) and count differences to the  $w = -1$  ( $\Lambda$ ) model (bottom panels) for objects with mass  $M > 10^{13}h^{-1}M_{\odot}$ . Panels on the left show results for homogeneous dark energy whereas panels on the right show the same models in the inhomogeneous dark energy case. Lines are the same as for Fig. 1.

and deficits at high redshift. All the other models give the opposite behaviour as their  $\delta_c/\sigma_8g$  is always lower than that of the  $w = -1$  model. Therefore, for  $w = -1.2$  we expect the integrated number counts to be larger than for the cosmological constant model until the redshift  $z_t$ . The remaining models must show the opposite behaviour. The difference between the integrated number counts of a model with respect to the cosmological constant must decrease with redshift for  $z > z_t$ . Eventually above a redshift  $z_{\text{flat}}$ , the integrated number counts should become constant with redshift because, as we have noted before, the number counts (Eq. (16)) decrease exponentially with redshift hence contributions above  $z_{\text{flat}}$  become negligible. Note that  $z_{\text{flat}}$  becomes progressively smaller for structures with larger mass limits ( $M_{\text{inf}}$ ) because a smaller number of these objects form at higher redshifts. This simply reflects the hierarchical nature of structure formation in models described by Eqs. (12)-(14). Models give quite different integrated count differences  $(N - N_{\Lambda})$  depending on the maximum redshift of integration. For homogeneous dark energy, maximum deviations from the  $\Lambda$ -model are generally obtained near  $z_t$  of the dominant class of structures, whereas for inhomogeneous dark energy maximum deviations generally occur at much higher redshifts,  $z \simeq z_{\text{flat}}$ .

In the inhomogeneous scenario, the interpretation of the redshift dependence of the integrated number counts is similar to that of the homogeneous case. As we have seen, the inhomogeneous case yields higher excesses and lower

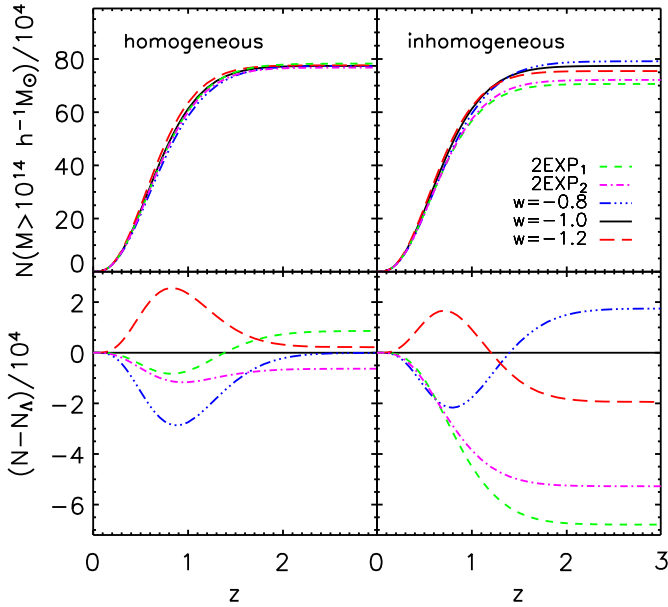


**Fig. 9.** Same as Fig. 8 for objects with mass  $M > 10^{14} h^{-1} M_{\odot}$ .

deficits for the  $w = -0.8$  model, hence we expect at high redshift, a positive difference in integrated counts compared to the cosmological constant model. This is quite visible in the right lower panels of Figs. 8 and 9. Through a similar argument, we expect at high redshift, a negative difference of integrated number counts with respect to the cosmological constant for the  $w = -1.2$  model. Moreover, because there are hardly any excesses in the 2EXP models, we must expect the difference of integrated number counts to flatten out at  $z_t$  at large negative values for these two models.

### 4.3. Normalisation

So far in this work we have normalised the various dark energy models such that they reproduce the abundance of dark matter halos at redshift zero (i.e. the local abundance) of a  $\Lambda$ -model with  $\sigma_8 = 0.9$ . However, observations that are being used to quantify the number of observed structures trace baryonic (emitting) gas and not dark matter halos directly. For systems where non-gravitational physics is important, i.e. the less massive structures, this may lead to an important miss-match between dark matter halos and emitting structure counts. Therefore, we dedicate the rest of this section to discuss the implications on our results of dropping the constraint of normalizing models to the same abundance at  $z = 0$ . Instead, we consider that all models have the same  $\sigma_8 = 0.9$  normalization, as given by present day observations (e.g. Spergel et al. 2003).

We illustrate the effects of inhomogeneous dark energy on one single mass bin. Figure 10 shows number counts in the mass bin  $10^{14} < M/(h^{-1} M_{\odot}) < 10^{15}$  and Fig. 11 the integrated number counts above mass  $M > 10^{14} h^{-1} M_{\odot}$ .

Both figures consider inhomogeneous dark energy models. In the left panels of these figures we are assuming that models are normalized to the same halo abundance at  $z = 0$  (i.e. same curves as those in the right panels of Figs. 5 and 9), whereas right panels assume that all models have a fixed normalisation,  $\sigma_8 = 0.9$ . Models in the homogeneous hypothesis have practically the same  $\sigma_8$  when they are normalized to the halo abundance at  $z = 0$ . Therefore we do not expect to observe much difference in the halo abundances from one dark energy model to another. The situation is quite different when dark energy is inhomogeneous. The comparison between panels in Fig. 10 indicates that fixing  $\sigma_8$  in all models causes much larger departures from the  $\Lambda$ -model than in the case where models are normalized to reproduce the same local halo abundances. At the maximum of  $\mathcal{N}^{\text{bin}}$ , the differences between dark energy models come from the fact that for a fixed  $\sigma_8$ , the mass function reflects the variations of  $\delta_c/g$  with  $z$ , which effects dominate those of the volume element in Eq. (15) for this mass bin. It is interesting to note that the structure of the curves can change dramatically depending whether we fix the local abundance or  $\sigma_8$ .

As this work was being completed Manera and Mota (2005) made public an analysis similar to the one presented here for the particular scenario of coupled quintessence. In their work, they have fixed  $\sigma_8$  for the two models under study rather than the local halo abundance. We have verified that indeed, also in the coupled quintessence model, the departures from a cosmological constant model are larger if one takes the former approach.

## 5. Conclusions

Number counts of collapsed structures are commonly proposed as a tool to probe dark energy models. In the simplest case of a constant equation of state, galaxy cluster number counts may constrain the dark energy, provided we have a good knowledge of the cluster physics and their redshifts (see for example Majumdar and Mohr (2004); Wang *et al.* (2004)). In the present study we have investigated, using the Press-Schechter mass function, two complications to the general picture: First, we have revisited the modifications introduced by a varying equation of state or by including a phantom component; second we have explored the effect of an inhomogeneous dark energy which collapses with the dark matter.

More specifically, we have considered a scalar potential built out of two exponential terms for which two sets of parameters (models 2EXP<sub>1</sub> and 2EXP<sub>2</sub>) were explored. Although their equations of state at present are almost indistinguishable, they undergo quite different evolutions at higher redshifts and generally give different results. In our analysis we have also included a phantom dark energy model ( $w = -1.2$ ), compatible with present observations. An interesting feature of phantom dark energy is that it induces opposite departures from the  $\Lambda$ -model as compared with the other models considered in this paper. That is,



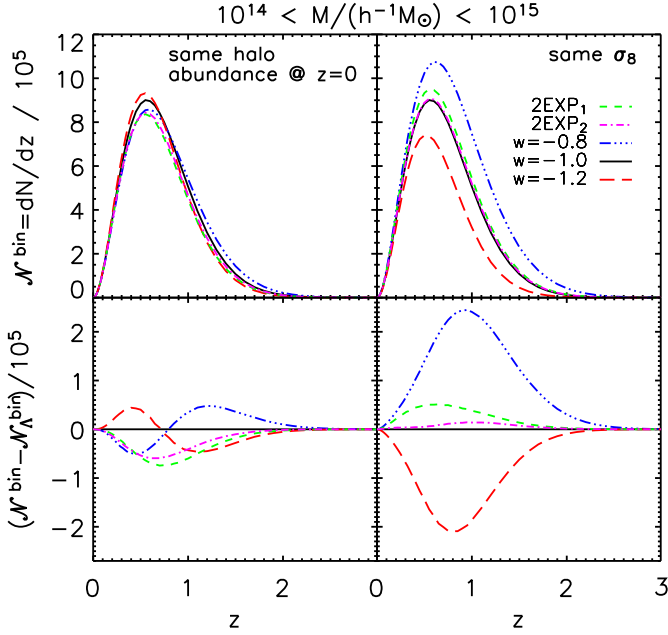


**Fig. 10.** Redshift dependence of number counts (top panels) and count differences relative to the  $\Lambda$ -model (bottom panels) for objects with mass within the  $10^{14} < M/(h^{-1}M_{\odot}) < 10^{15}$ , assuming dark energy is inhomogeneous. Panels on the left show results assuming models are normalized to the same halo abundance at  $z = 0$ , whereas panel on the right assume that models have all  $\sigma_8 = 0.9$  (which implies different halo abundances at  $z = 0$ , see text). Lines are the same as in Fig. 1.

we expect an excess of sources in a phantom energy model when other models predict a deficit.

Recently Mota and van de Bruck (2004) proposed that dark energy may cluster in forming structures (inhomogeneous dark energy). They have investigated the growth and collapse of cosmological structures under the inhomogeneous hypothesis. Going a step forward, we have investigated in the present study the implications of this hypothesis on the number density of collapsed objects. We have found that inhomogeneous dark energy generally enhances departures from the  $\Lambda$ -model. This includes the models with a time varying equation of state, which can present several times larger departures (from the  $\Lambda$ -model) as compared to the homogeneous case. Yet our results indicate that the inhomogeneous dark energy hypothesis causes maximum deviations no larger than  $\sim 15\%$  in mass bins with comfortably large numbers of collapsed halos. Another interesting feature is that maximum departures from the  $\Lambda$ -model are generally obtained at higher redshift for inhomogeneous dark energy than for the homogeneous case, which generally show maximum departures near the maximum of  $\mathcal{N}^{\text{bin}}(z)$ . This may be a helpful feature to test for the inhomogeneous hypothesis. Larger departures from the  $\Lambda$ -model are also stronger for the more massive structures, but these are quite rare objects, which makes it difficult to statistically distinguish between models. Our

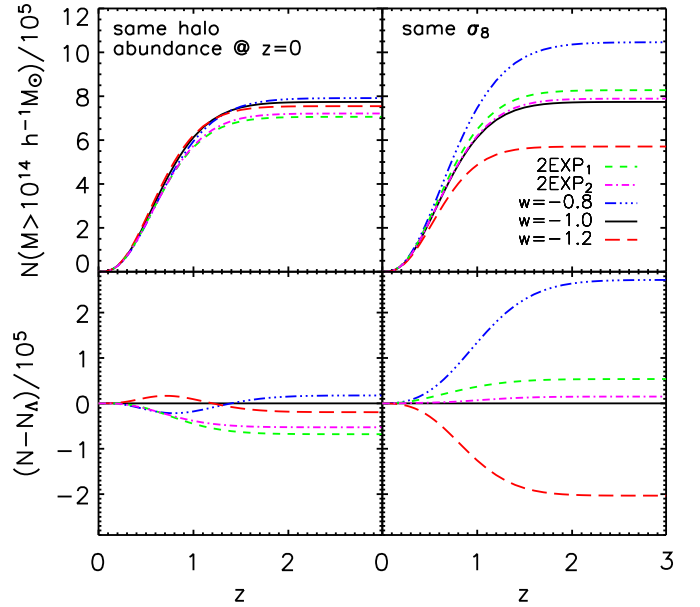


**Fig. 11.** Integrated number counts up to redshift  $z$  (top panels) and integrated count differences relative to the  $\Lambda$ -model (bottom panels) for objects with mass above  $10^{14}h^{-1}M_{\odot}$ , assuming dark energy is inhomogeneous. Panels on the left show results assuming models are normalized to the same halo abundance at  $z = 0$ , whereas panels on the right assume that models have all  $\sigma_8 = 0.9$ . Lines are the same as in Fig. 1.

analysis reveals that the inhomogeneous dark energy hypothesis has the greatest impact on the 2EXP1 model.

In this work, we have assumed that the matter transfer function remains unchanged at cluster scales. We have further assumed that models are normalized to reproduce the same abundance of dark matter halos at redshift zero. In the homogeneous hypothesis all models have practically the same  $\sigma_8$  and there are not much differences in the halo abundances from one dark energy model to another. When dark energy is inhomogeneous,  $\sigma_8$  differ by a few percent and the departures from the  $\Lambda$ -model are much larger. It is, however, worth noting that the gas physics which rules the observed quantities adds a degree of degeneracy. We have evaluated the effects of alternatively fixing  $\sigma_8$  to a specific value regardless of the dark energy model. In this case we verified that the departures from a  $\Lambda$  cosmology are further enhanced.

Our results show that constraining dark energy models from structure counts is complicated when models have time varying equation of state. It becomes an even more complicated task when the possibility of inhomogeneous dark energy is taken into account. Therefore in order to constrain dark energy models, we need to explore as many observable quantities as possible. Our results suggest that besides redshift distribution of structures, considering structures in mass ranges significantly increases the number of observables. Indeed, each theoretical model provides specific predictions for the redshift

evolution of number counts and integrated count differences in different mass bins. The comparison of such quantities with observations can be used for testing models against observational data. It may further allow to distinguish between homogeneous and inhomogeneous dark energy models. However, this requires good knowledge of the gas physics, redshifts of observed structures and, more precisely, a good understanding of the selection function of the observations.

*Acknowledgements.* We thank David Mota and Morgan LeDelliou for invaluable discussions. NJN is supported by the Department of Energy under contract DE-FG02-94ER40823 at the University of Minnesota. AdS acknowledges support by CMBnet EU TMR network and Fundação para a Ciência e Tecnologia under contract SFHR/BPD/20583/2004, Portugal. This work was partly supported by CNES. We would like to thank the referee for his/her comments.

## References

- Amendola, L., 2000, *Phys. Rev. D* **62**, 043511.
- Amendola, L., 2003, [astro-ph/0311175](#).
- Arbey, A., J. Lesgourgues, and P. Salati, 2001, *Phys. Rev. D* **64**, 123528.
- Armendariz-Picon, C., V. Mukhanov, and P. J. Steinhardt, 2000, *Phys. Rev. Lett.* **85**, 4438.
- Baccigalupi, C., S. Matarrese, and F. Perrotta, 2000, *Phys. Rev. D* **62**, 123510.
- Bagla, J. S., H. K. Jassal, and T. Padmanabhan, 2003, *Phys. Rev.* **D67**, 063504.
- Barreiro, T., E. J. Copeland, and N. J. Nunes, 2000, *Phys. Rev. D* **61**, 127301.
- Battye, R. A., and J. Weller, 2003, *Phys. Rev.* **D68**, 083506.
- Bean, R., and J. Magueijo, 2002, *Phys. Rev.* **D66**, 063505.
- Blanchard, A., M. Douspis, M. Rowan-Robinson, and S. Sarkar, 2003, *Astron. Astrophys.* **412**, 35.
- Brax, P., and J. Martin, 1999, *Phys. Lett. B* **468**, 40.
- Caldwell, R. R., 1999, [astro-ph/9908168](#).
- Cole, S., *et al.* (The 2dFGRS), 2005, [astro-ph/0501174](#).
- Ferreira, P. G., and M. Joyce, 1997, *Phys. Rev. Lett.* **79**, 4740.
- Haiman, Z., J. J. Mohr, and G. P. Holder, 2001, *ApJ* **553**, 545.
- Horellou, C., and J. Berge, 2005, *Mon. Not. Roy. Astron. Soc.* **360**, 1393.
- Kamenshchik, A. Y., U. Moschella, and V. Pasquier, 2001, *Phys. Lett.* **B511**, 265.
- Klypin, A., A. V. Maccio, R. Mainini, and S. A. Bonometto, 2003, *Astrophys. J.* **599**, 31.
- Kuhlen, M., L. E. Strigari, A. R. Zentner, J. S. Bullock, and J. R. Primack, 2004, [astro-ph/0402210](#).
- Linder, E. V., and A. Jenkins, 2003, [astro-ph/0305286](#).
- Lokas, E. L., P. Bode, and Y. Hoffman, 2003, [astro-ph/0309485](#).
- Ma, C.-P., R. R. Caldwell, P. Bode, and L.-M. Wang, 1999, *Astrophys. J.* **521**, L1.
- Majumdar, S., and J. J. Mohr, 2004, *Astrophys. J.* **613**, 41.
- Manera, M., and D. F. Mota, 2005, [astro-ph/0504519](#).
- Maor, I., and O. Lahav, 2005, [astro-ph/0505308](#).
- Mohr, J. J., 2004, [astro-ph/0408484](#).
- Mota, D. F., and C. van de Bruck, 2004, [astro-ph/0401504](#).
- Nunes, N. J., and D. F. Mota, 2004, [astro-ph/0409481](#).
- Padmanabhan, T., 1993, *Structure formation in the universe* (Cambridge, UK: Cambridge University Press, —c1993).
- Padmanabhan, T., and T. R. Choudhury, 2002, *Phys. Rev.* **D66**, 081301.
- Perlmutter, S., *et al.* (Supernova Cosmology Project), 1999, *Astrophys. J.* **517**, 565.
- Perrotta, F., and C. Baccigalupi, 2002, [astro-ph/0201335](#).
- Press, W. H., and P. Schechter, 1974, *Astrophys. J.* **193**, 437.
- Ratra, B., and P. J. E. Peebles, 1988, *Phys. Rev. D* **37**, 3406.
- Riess, A. G., *et al.* (Supernova Search Team), 1998, *Astron. J.* **116**, 1009.
- Riess, A. G., *et al.*, 2004, [astro-ph/0402512](#).
- Romer, A. K., P. T. P. Viana, A. R. Liddle, and R. G. Mann, 2001, *ApJ* **547**, 594.
- Ruhl, J. E., *et al.* (The SPT), 2004, [astro-ph/0411122](#).
- Sahni, V., 2004, [astro-ph/0403324](#).
- Shanks, T., 2004, [astro-ph/0401409](#).
- Spergel, D. N., *et al.* (WMAP), 2003, *Astrophys. J. Suppl.* **148**, 175.
- Uzan, J.-P., 1999, *Phys. Rev. D* **59**, 123510.
- Viana, P. T. P., and A. R. Liddle, 1996, *Mon. Not. Roy. Astron. Soc.* **281**, 323.
- Wang, S., J. Khoury, Z. Haiman, and M. May, 2004, *Phys. Rev.* **D70**, 123008.
- Weinberg, N. N., and M. Kamionkowski, 2002, [astro-ph/0210134](#).
- Weller, J., R. Battye, and R. Kneissl, 2002, *Phys. Rev. Lett.* **88**, 231301.
- Wetterich, C., 1988, *Nucl. Phys. B* **302**, 668.
- Zlatev, I., L.-M. Wang, and P. J. Steinhardt, 1999, *Phys. Rev. Lett.* **82**, 896.